Title

Conservative Tryptophan Mutants of the Protein Tyrosine Phosphatase YopH Exhibit Impaired WPD-Loop Function and Crystallize with Divanadate Esters in Their Active Sites

Journal

Biochemistry, 54(42)

ISSN

0006-2960

Authors

Moise, Gwendolyn
Gallup, Nathan M
Alexandrova, Anastassia N
et al.

Publication Date

2015-10-27

DOI

10.1021/acs.biochem.5b00496

Peer reviewed

BIOCHEMISTRY
including biophysical chemistry & molecular biology

Article

pubs.acs.org/biochemistry

Conservative Tryptophan Mutants of the Protein Tyrosine Phosphatase YopH Exhibit Impaired WPD-Loop Function and Crystallize with Divanadate Esters in Their Active Sites

Gwendolyn Moise,[†] Nathan M. Gallup,[‡] Anastassia N. Alexandrova,[‡,§] Alvan C. Hengge,*[,†] and Sean J. Johnson*[,†]

[†]Department of Chemistry and Biochemistry, Utah State University, Logan, Utah 84322-0300, United States
[‡]Department of Chemistry and Biochemistry, University of California, Los Angeles, California 90095-1569, United States
[§]California Nanosystems Institute, University of California, Los Angeles, California 90095-1569, United States

Supporting Information

ABSTRACT: Catalysis in protein tyrosine phosphatases (PTPs) involves movement of a protein loop called the WPD loop that brings a conserved aspartic acid into the active site to function as a general acid. Mutation of the tryptophan in the WPD loop of the PTP YopH to any other residue with a planar, aromatic side chain (phenylalanine, tyrosine, or histidine) disables general acid catalysis. Crystal structures reveal these conservative mutations leave this critical loop in a catalytically unproductive, quasi-open position. Although the loop positions in crystal structures are similar for all three conservative mutants, the reasons inhibiting normal loop closure differ for each mutant. In the W354F and W354Y mutants, steric clashes result from six-membered rings occupying the position of the five-membered ring of the native indole side chain. The histidine mutant dysfunction results from new hydrogen bonds stabilizing the unproductive position. The results demonstrate how even modest modifications can disrupt catalytically important protein dynamics. Crystallization of all the catalytically compromised mutants in the presence of vanadate gave rise to vanadate dimers at the active site. In W354Y and W354H, a divanadate ester with glycerol is observed. Such species have precedence in solution and are known from the small molecule crystal database. Such species have not been observed in the active site of a phosphatase, as a functional phosphatase would rapidly catalyze their decomposition. The compromised functionality of the mutants allows the trapping of species that undoubtedly form in solution and are capable of binding at the active sites of PTPs, and, presumably, other phosphatases. In addition to monomeric vanadate, such higher-order vanadium-based molecules are likely involved in the interaction of vanadate with PTPs in solution.

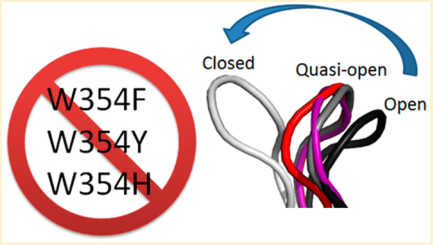

Protein tyrosine phosphatases (PTPs) catalyze the dephosphorylation of Tyr residues, functioning in concert with protein tyrosine kinases (PTKs) to modulate signal transduction pathways.[1−4] One of the most-studied PTPs is the *Yersinia* protein tyrosine phosphatase YopH. YopH is an essential virulence factor in *Yersinia*, a bacterial genus that includes three species causative of human illness, ranging from gastrointestinal disease to bubonic plague.[5] YopH is also one of the most powerful phosphatases known, with k_{cat} values of ∼1300 s^{-1} for physiological phosphopeptide substrates at 30 °C.[6,7] Given the rate constant of $\sim 10^{-20}$ s^{-1} for the uncatalyzed hydrolysis of phosphate monoester dianions, YopH is one of the most efficient enzymes known.[8] Another well-studied PTP is PTP1B, a human phosphatase with a number of roles that include regulation of the insulin receptor protein. PTP1B and YopH have highly superimposable active sites and the same mechanism, although catalysis by PTP1B is 1 order of magnitude slower.

PTPs catalyze the hydrolysis of tyrosine phosphate esters by a two-step mechanism (Figure 1) via a phosphoenzyme intermediate.[2,3] The phosphoryl group binds in a conserved element known as the P-loop, a signature motif with the sequence CX_5R that includes the nucleophilic cysteine, a conserved arginine, and a semicircular arrangement of backbone amide groups. Substrate binding in PTPs favors the closed conformation of a flexible loop bearing the conserved sequence WPD. This loop contains a conserved aspartic acid that functions as a general acid in the first chemical step, and as a general base in the second (Figure 1).[9,10] In the closed conformation, the WPD loop brings the conserved Asp residue up to 8 Å closer to the bound substrate.[11−15] Although the open- and closed-loop forms of the active sites of YopH and PTP1B superimpose well with one another, the loops move at significantly different rates in the two enzymes and respond differently to mutation of the W residue.[16] The W354F mutant of YopH has lost general acid catalysis and crystallizes with this loop in an intermediate, quasi-open position. In contrast, the corresponding W179F mutation in PTP1B has no significant structural effect, and causes a minor reduction in rate.[17]

Received: May 5, 2015
Revised: October 7, 2015

DOI: 10.1021/acs.biochem.5b00496
Biochemistry XXXX, XXX, XXX−XXX

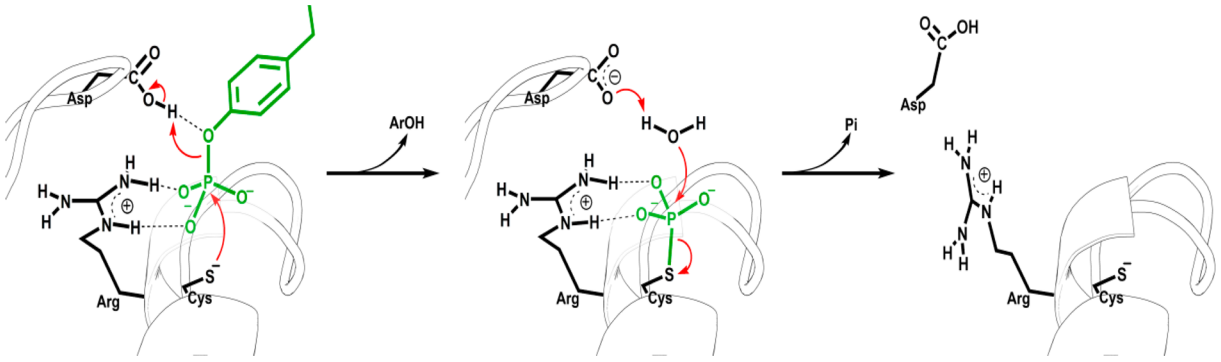

Figure 1. Mechanism of hydrolysis by protein tyrosine phosphatases (PTPs). In the first step, nucleophilic attack by a conserved cysteine is concerted with leaving group departure and protonation by aspartic acid. Subsequent hydrolysis of the phosphocysteine intermediate regenerates free enzyme.

Crystal structures of the W354F mutant of YopH obtained in the presence and absence of ligands show the same quasi-open loop position. Furthermore, a structure obtained with vanadate revealed a bridged divanadate molecule at the active site.[18] Such a species would be rapidly hydrolyzed by general acid catalysis in the native enzyme, leaving behind the monomeric form typically observed in the active sites of phosphatases crystallized in the presence of vanadate. Thus, the loop-compromised mutant permitted the visualization of a vanadate species that likely forms and competes with substrate in solution but has not been observed in crystals of a functional phosphatase. The W354F instance was the first such example of which we are aware.

We report here results with two additional mutations to YopH that also impair the WPD loop and disable general acid catalysis. Crystals of these enzymes show the presence of an ester complex formed between divanadate and glycerol; the latter was added only after crystallization, as a cryoprotectant. These results demonstrate that vanadate oligomers bind to PTPs, and that interactions with ester-forming molecules in solution can rapidly result in new species bound at the active site. Previous studies have shown that effects from confinement, and local interactions with membrane interfaces, have effects on the coordination chemistry of vanadium.[19,20] It is, therefore, not surprising that an active site environment can provide stabilization to species that cannot be observed in solution. A computational analysis of the bonding in the divanadate glycerol ester was performed to examine how it differs from analogous complexes in small molecule crystals and compared to divanadate alone. The results provide insight into the effect of the active site environment on the formation and stability of such species.

Together, the results reported here give new insights into how even conservative mutations affect WPD-loop movement in YopH, provide new examples of oligomeric vanadate species that can form and occupy the active site of PTPs, and reveal how the local environment affects the chemical bonding of such species. The computational results permit a comparison of how bonding within the divanadate moiety is affected by coordination with glycerol and how these protein-bound species compare with analogous structures found in the small molecule crystal database.

MATERIALS AND METHODS

Chemicals. IPTG and DTT were purchased from GoldBio. All other buffers and reagents were purchased from Sigma-Aldrich. *p*-Nitrophenyl phosphate (*p*-NPP) was made and purified as previously described.[21] Crystal trays and coverslips were purchased from Hampton Research.

Protein Expression and Purification. The YopH mutants were made using the Qiagen QuikChange Lightning Site-directed Mutagenesis Kit. Primers were designed according to directions in the protocol. The W354Y and W354H mutations were introduced using complementary primers where the primers in the forward direction were GTG GTT CAT GTT GGC AAT T**AT** CCC GAT CAG ACC GCA GTC AGC and G GTT CAT GTT GGC AAT **CAT** CCC GAT CAG ACC GCA GTC AGC TCT G, respectively. Both mutants were expressed and purified as previously described and showed 99% purity on a sodium dodecyl sulfate−polyacrylamide gel electrophoresis gel.[18]

Crystallography. Crystals were grown by hanging drop vapor diffusion at room temperature (22 °C). Crystals of YopH mutants W354H and W354Y were grown with a well solution of 0.1 M HEPES buffer (pH 7.5) and 15−28% polyethylene glycol (PEG) 3350. The crystals grew best in the higher PEG concentration range (20−26%), but crystals can be seen throughout the range. The drop consisted of 2 μL of well solution and 3 μL of protein solution (15 mg/mL enzyme in 100 mM sodium acetate, 100 mM NaCl, 1 mM EDTA, and 1 mM DTT). Crystals appeared in 3−5 days. Crystal optimization was achieved by microseeding. Crystals were prepared for cryocooling by being transferred into a stabilization solution containing increasing concentrations of glycerol, starting at 0% and increasing by 5% increments to a final concentration of 20% (5 min/step). The crystals were then flash-frozen in liquid nitrogen and stored under liquid nitrogen.

Crystals in complex with vanadate were grown by incubating protein with sodium metavanadate (Na_3VO_4) at a 1:5 molar ratio, where protein/Na_3VO_4 solution was left to interact for 30 min on ice prior to cocrystallization. A stock solution of Na_3VO_4 was made up to a concentration of 106.4 mM in dilute NaOH as previously described[22] and mixed with the protein solution, and then the combined solution was added to the drop. The concentration of the sodium metavanadate solution was checked by UV spectroscopy at 260 nm.[23] Vanadate-bound crystals grew best in the lower PEG concentration range (16−20%), and microseeding was required to obtain crystals.

Data Collection and Validation. Crystals were screened on a home source X-ray system, and diffraction data were collected at the Stanford Radiation Lightsource (SSRL). Data

DOI: 10.1021/acs.biochem.5b00496
Biochemistry XXXX, XXX, XXX−XXX

Table 1. Data Collection and Refinement Statistics for W354Y and W354H YopH Ligand-Free and Cocrystallized Oxyanion-Bound Forms

	W354Y		W354H	
	ligand-free	V_2O_7	ligand-free	V_2O_7
	Data Collection			
beamline	SSRL 7-1	SSRL 7-1	SSRL 7-1	SSRL 7-1
wavelength (Å)	0.97946	0.97946	0.97946	0.97946
space group	$P2_12_12_1$	$P2_12_12_1$	$P2_12_12_1$	$P2_12_12_1$
unit cell dimensions [a, b, c (Å); $\alpha = \beta = \gamma = 90°$]	52.9, 60.5, 89.4	54.4, 58.0, 90.5	53.3, 60.6, 89.3	52.8, 60.4, 89.3
resolution range (Å)	50.0−1.05	50.0−1.12	40.0−1.20	50−1.12
outer shell (Å)	1.09−1.05	1.16−1.12	1.24−1.20	1.16−1.12
no. of reflections				
unique	133901	106319	90707	109639
total	1495665	1071240	1281329	1253588
average redundancy	8.9	10.1	14.1 (12.5)	11.4 (10.5)
mean $I/\sigma(I)$	48.3 (4.7)	46.7 (6.1)	24.9 (5.2)	52.8 (10.4)
completeness (%)	99.7 (100.0)	96.2 (78.0)	99.4 (97.4)	99.4 (99.2)
R_{merge} (%)	0.036 (0.414)	0.040 (0.218)	0.096 (0.53)	0.064 (0.723)
	Refinement			
R_{work}, R_{free} (%)	0.128, 0.140	0.129, 0.145	0.140, 0.159	0.141, 0.159
no. atoms in the structure				
total	5295	5005	5039	4996
protein	4839	4530	4644	4586
waters/solvent	456	457	395	392
ligands/ions	0	18	0	18
B factor (Å^2)				
average	14.83	15.48	18.56	20.01
protein	12.40	12.92	15.99	17.49
water/solvent	27.91	28.34	33.75	34.67
ligand	–	23.26	–	18.25
root-mean-square deviation for bonds (Å)	0.008	0.009	0.009	0.008
root-mean-square deviation for bond angles (deg)	1.32	1.28	1.35	1.29
protein geometry				
Ramachandran outliers (%)	0.0	0.0	0.0	0.0
Ramachandran favored (%)	98.17	97.3	97.9	98.3
rotamer outliers (%)	0.0	0.0	0.0	0.8
PDB entry	4YAA	4ZN5	4Z6B	4ZI4

were processed using HKL2000.[24] Molecular replacement was performed with Phaser[25](as implemented in either CCP4[26]or Phenix[27]) using wild-type (WT) YopH [Protein Data Bank (PDB) entry 1YPT][28] as a search model. Model building, refinement, and validation were performed using Coot,[29] Phenix,[30] and MolProbity[31] (Table 1). The structures are deposited as PDB entries 4ZN5, 4YAA, 4ZI4, and 4Z6B. Pymol[32] was used to align structures and create figures.

Kinetics. The pH−rate profiles for WT YopH and both mutants were collected using real-time and end point kinetics in the pH range of 4.5−8.5 with the substrate *p*-NPP. The conditions were 0.1 M buffer base mix (100 mM sodium acetate, 100 mM Tris, and 100 mM HEPES). Substrate concentrations ranged from $^1/_8K_M$ to $5K_M$. Unless otherwise specified, inhibition experiments were conducted at the pH optimum of 5.5 at 23 °C in a 96-well plate in 100 mM acetate buffer and 100 mM sodium chloride with 1 mM DTT. The vanadate inhibitor concentrations ranged from 0.01 to 5.0 μM. Substrate concentrations ranged from 0.30 to 12 mM *p*-NPP. Formation of *p*-nitrophenol from *p*-NPP was assayed at 400 nm using a VersaMax 96-well microplate reader. End point reactions were quenched with the addition of 10 N NaOH after reaction times ranging from 1.5 to 30 min. Glycerol inhibition experiments were conducted using a vanadate concentration of 32 μM at pH 5.5 with concentrations of glycerol from 0 to 275 mM (Figure S3). Enzyme concentrations in stock solutions were determined using a NanoDrop ND-1000 spectrophotometer.

Computational Methods. For both W354F and W354Y, the relevant region was extracted from the enzyme for computational study. This region consisted of residues that interacted directly with the vanadate and vanadate−glycerol complexes, as well as charged and polar residues in the proximity that may provide electrostatic influences. Hydrogen atoms were added using Chimera,[33] while protons on the vanadate complex were added by hand using Avogadro.[34] All protonation states of amino acids were assumed, while the coordinating Cys in both W354F and W354Y was assumed to be deprotonated, as well as the coordinating oxygens contributed by glycerol in W354Y. The truncated complexes consisted of approximately 150 atoms each. The spin states were considered to be singlets, assuming the d subshell in V to be empty. Natural bond orbital (NBO) analysis[34−38] at the B3LYP[39−41]/TZVP[42] level of theory was used to evaluate the chemical bonding in the complexes. Optimizations were performed using Turbomole version 6.3[43] using the similar def2-TZVP basis set.[44,45] To accelerate calculations, the Resolution of Identity (RI)[46] and Multipole Accelerated

DOI: 10.1021/acs.biochem.5b00496
Biochemistry XXXX, XXX, XXX−XXX

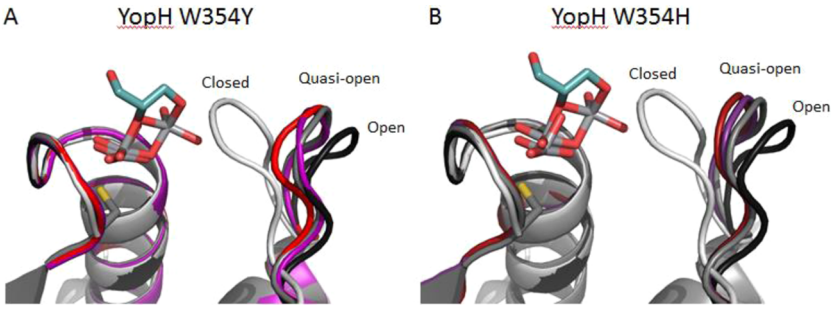

Figure 2. Comparison of WT YopH with mutants W354Y (A) and W354H (B) with vanadate (WT) or divanadate glycerol ester (mutants). The ligand-free, open-loop WT YopH is colored black and the vanadate-bound, closed-loop WT YopH light gray. The W354F mutant, with its loop in a quasi-open position, is colored dark gray. (A) The ligand-free W354Y structure is colored purple, and the divanadate glycerol ester-bound form is colored red. (B) The ligand-free W354H structure is colored purple, and the divanadate glycerol ester-bound form is colored red. The ligand-bound forms of both W354Y and W354H show the WPD loop in an unproductive quasi-open position, consistent with kinetic results.

Resolution of Identity (MARI-J)[47] were used. Empirical dispersion was included,[48] and solvent was included via the Conductor-like Screening Model (COSMO)[49] with a dielectric constant of 20, because the complexes are partially solvent accessible. NBO calculations were performed using the Gaussian 09 suite of programs.[50,51] Several protonation states were tested for both enzymes. For W354F, protonation on O4, O5, and O7 was attempted; however, only O5 was able to be successfully converged. The rest were not found to be minima and resulted in ring breaking upon optimization from various protonation configurations. For W354Y, protonation on O5 and O6 was attempted but was found to have an energetic difference of <1 kcal/mol, within the inherent error of density functional theory.

RESULTS

Comparison of the WPD-Loop Positions in W354Y and W354H with One Another, and with Previous Structures of W354F and WT. The crystal structures of W354H, with and without a bound ligand, showed the WPD loop in a quasi-open position (Figure 2) similar to that previously reported for the W354F mutant.[18] A very similar position is found for the WPD loop in the W354Y mutant, with only slight variation of the loop's configuration in the ligand-free structure.

Steady State Kinetics for W354H and W354Y. The W354H and W354Y mutants exhibit Michaelis–Menten saturation kinetics with the substrate *p*-NPP, though at a rate significantly reduced relative to that of WT YopH. The k_{cat} values at 23 °C for the W354H and W354Y mutants at pH 5.5 are 5.2 ± 0.6 and 2.3 ± 0.1 s^{-1}, respectively, compared with 720 ± 5 s^{-1} for WT. The pH optimum is 5.5 for WT and W354H, whereas the W354Y mutant has a slightly shifted pH optimum of 6.2, where its k_{cat} is 6.5 ± 0.9 s^{-1} (Figure 3, bottom panel). The K_M values for the W354H and W354Y mutants at pH 5.5 are 7.07 ± 1 and 6.4 ± 0.9 mM, respectively, higher than the K_M of 1 mM for WT. In both mutants, the basic limb of the pH–rate profile is largely lost, with the rate above the maximum dropping off only slightly before leveling off (Figure 3). This is consistent with previously reported data for the W354F mutant, in which the general acid D356 is no longer fully functional.[18,52]

Observation of Divanadate Glycerol Esters at the Active Sites of W354H and W354Y. The YopH W354H and W354Y crystals grown in the presence of vanadate showed electron density consistent with a divanadate species. A similar

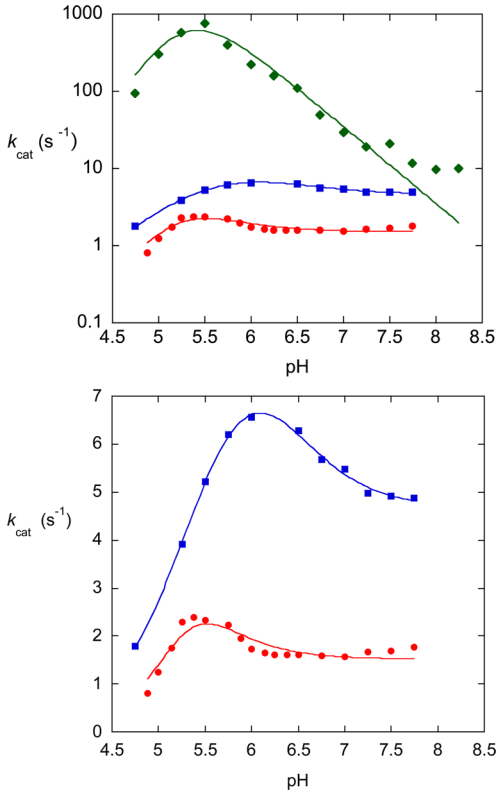

Figure 3. Effects of pH on the hydrolysis of *p*-NPP by YopH mutants W354Y and W354H compared to WT YopH at 23 °C. The W354Y data are shown as blue squares, W354H data as red circles, and WT data as green diamonds. The top panel shows the comparative k_{cat} values in the mutants compared to those of WT YopH are lower by >2 orders of magnitude, and the basic limb of the pH profile is lost. The bottom panel shows that the mutant kinetic data decrease only slightly at pH values above their respective maxima, similar to previous data reported for the W354F mutant.[18]

divanadate moiety was previously observed in the W354F mutant.[18] However, the electron density in the YopH W354H and W354Y structures also showed the presence of a glycerol molecule with two oxygen atoms occupying coordination sites (Figure 4). In the divanadate glycerol ester, atom V1 is coordinated to the sulfur atom of cysteine C401. Atoms O1 and O2 are hydrogen bonded to backbone amide N–H groups of P-loop residues R402, A403, V405, and G406. Atom O3 bridges V1 and V2 and is hydrogen bonded to the backbone

DOI: 10.1021/acs.biochem.5b00496
Biochemistry XXXX, XXX, XXX–XXX

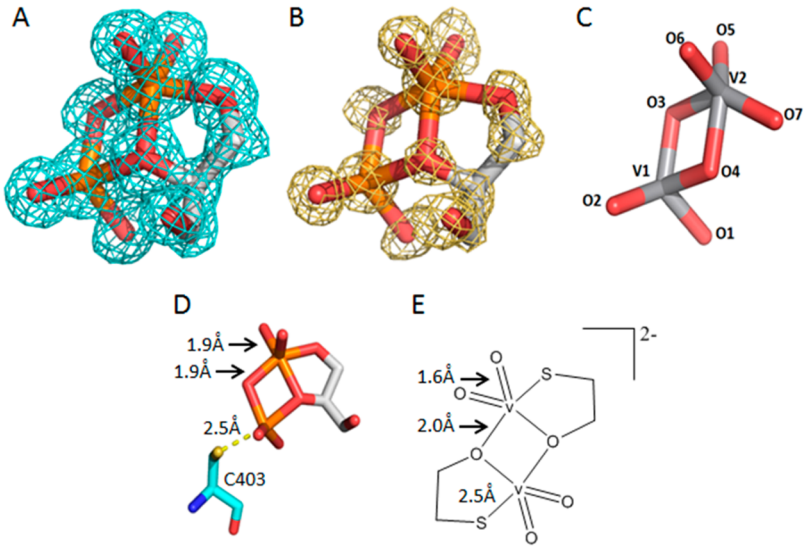

Figure 4. Structural comparisons of the divanadate glycerol ester observed in the active site of W354Y with other divanadate species. (A) $2F_o - F_c$ electron density map for the divanadate glycerol ester in the active site of W354Y at the 1.0σ contour level. The divanadate ester in W354H is identical. (B) Simulated annealing omit map at the 1.0σ contour level calculated with the divanadate ester omitted from the model. (C) Divanadate previously seen in YopH W354F. (D) Bond distances for each type of bond are shown in angstroms, with a length of 2.5 Å for the S−V bond and 1.9 Å for indicated V−O bonds. (E) For comparison, a known small molecule divanadate[71] is shown with bond distances for corresponding bonds in angstroms.

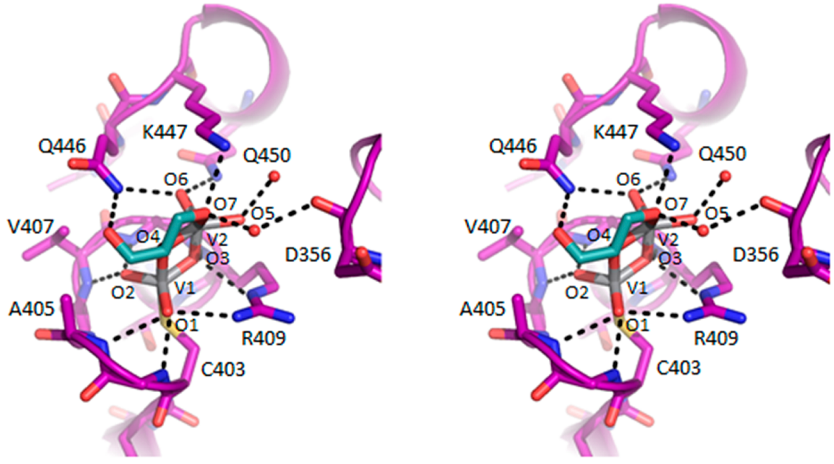

Figure 5. Stereo figure showing the hydrogen bond network in the active site of the W354Y mutant with the divanadate glycerol ester bound. The hydrogen bonds are shown as dashed black lines where the distances are between 2.8 and 3.1 Å. Vanadate atoms are colored gray; the glycerol ester is colored teal, and the enzyme is colored pink. The hydrogen bond network stabilizes the divanadate glycerol ester.

amide and the ε-nitrogen of R409. Atoms O5 and O6 are the terminal oxygen atoms bonded to V2. The crystals were grown at pH 7.5, making it likely that either O5 or O6 is protonated. In the crystal, O5 is hydrogen bonded to two water molecules while O6 is hydrogen bonded to the amide N−H of residues Q446 and Q450 with a distance of 2.9 Å (Figure 5). Therefore, O5 is assumed to be protonated and O6 not. Compared to the dimeric vanadate in the W354F structure (Figure 4C), in the glycerol esters found in this work, atoms O4 and O7 have been replaced by oxygen atoms from the glycerol ester where O4 is the bridging atom between V1 and V2 and O7 is bonded to V2. The electron density map in Figure 4A shows a gap between atom O7 and V2.

Bonding Differences of the Divanadate Core in the Glycerol Ester. The divanadate core in the glycerol ester structure (Figure 4A) is generally similar to the previously reported structure of divanadate alone in the W354F mutant (Figure 4C), but there are significant differences in some bond angles between oxygen and vanadate, as shown in Table 2. Overall, the W354F divanadate has a more flattened geometry in the terminal oxygens. The position of O5 is different in the glycerol ester, farther from the bridging O3 atom and closer to the glycerol O7 atom.

Kinetics in the Presence of Vanadate and Added Glycerol. The inhibition by vanadate of YopH W345H with the substrate *p*-NPP was measured in the presence of 0−275 mM glycerol. Glycerol alone does not inhibit YopH W354H (Figure S3), and added glycerol did not enhance inhibition by vanadate. The k_{cat} at 32 μM vanadate ($10K_i$) was 0.071 s^{-1} in the absence of glycerol and did not significantly change over the glycerol concentration range tested (Figure S3).

Computational Analysis of Vanadate Complexes. The divanadate glycerol ester of W354Y found in this study, and the divanadate complex found in a previous study of the W354F

DOI: 10.1021/acs.biochem.5b00496
Biochemistry XXXX, XXX, XXX−XXX

Table 2. Comparison of the Angles of the Oxygen Bonds around the Second Vanadium in the Divanadate Structure and the Divanadate Glycerol Structure[a]

angles	W354F	W354Y	difference
O_3-V_2-O_5	69.4	94.4	-25
O_5-V_2-O_6	103.5	105.1	-1.6
O_5-V_2-O_7	129.5	89.9	39.6
O_3-V_2-O_6	106.2	108.5	-2.3
O_4-V_2-O_6	101.1	104.5	-3.4
O_4-V_2-O_7	67.2	79.3	-12.1
O_6-V_2-O_7	101.4	106.2	-4.8

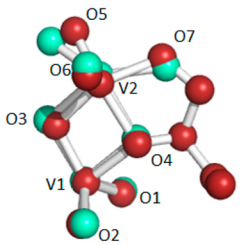

[a]On the right are the overlaid structures of the divanadate complexes shown in panels A (W354Y, red) and C (W354F, cyan) of Figure 4.

mutant, were analyzed computationally. The glycerol ester was modeled assuming protonation on either O5 or O6; however, as described above, on the basis of hydrogen bonds observed in the crystal, protonation on O5 is more likely. In the simple divanadate complex of W354F, protonation was modeled on O5. Table 3 outlines the nature of chemical bonding within each complex. The inconsistent nature of the bond populations suggests significant delocalization within the ring, which precipitates numerical error using NBO analysis. NBO's inability to characterize this delocalization is best illustrated by the alleged existence of four lone pairs on O4 in the W354F complex. The decreasing populations of each respective orbital

Table 3. Electronic Structure Parameters Characterizing the Vanadium and the Core Oxygen Atoms of the Vanadate Complexes Shown in Panels A and C of Figure 4[a]

	W354Y (O5 protonated)	W354Y (O6 protonated)	W354F (O5 protonated)
Q(V1)	0.47465	0.48708	0.53678
Q(V2)	0.76664	0.75449	0.67021
Q(O3)	−0.58994	−0.58636	−0.71285
Q(O4)	−0.50702	−0.52930	−0.57151
Q(S)	−0.08888	−0.12353	−0.32647
	Bond Population (|e|)		
V1−S σ	1.83403	1.87050	1.92570
V1−S π	1.88443	none	none
V1−O3 σ	1.82461	1.86361	1.94333
V1−O3 π	none	none	1.84156
V1−O4	1.87661	1.91441	none
V2−O3 σ	1.87459	1.87481	1.88011
V2−O3 π	1.81815	none	none
V2−O4	1.89713	1.89748	none
	Lone Pair Populations (|e|)		
LP1(O3)	1.80911	1.82386	1.84984
LP2(O3)	none	1.67226	none
LP1(O4)	1.86524	1.85103	1.82748
LP2(O4)	none	none	1.69656
LP3(O4)	none	none	1.58339
LP4(O4)	none	none	1.45719
LP1(S)	1.93562	1.93217	1.95739
LP2(S)	none	1.80825	1.88237

[a]The structure in Figure 4A is a glycerol ester, while that in Figure 4C is only the divanadate core. The identity of the protonated oxygen atom is given in the top row. Calculated with NBO analysis showing atomic charges (Q) and electronic populations of two-center, two-electron bonds and lone pairs. A complete table including results for all the oxygen atoms appears in the Supporting Information.

suggest the presence of a highly ionic oxygen atom. Results have also been shown to be dependent on basis set, also suggesting a failure to accurately characterize delocalization in the ring.

DISCUSSION

All Conservative Mutations of W354 in YopH Compromise General Acid Catalysis. Published crystal structures of native WT YopH with an oxyanion ligand bound have the WPD loop closed over the active site, in the catalytically active position.[53] In contrast, WT structures with no bound ligand show the WDP loop in an open position (Figure 2).[53] It was previously found that the W354F mutant crystallizes with the WPD loop in a quasi-open position, in which the top of the loop has shifted only ∼2.0 Å from the open WPD loop toward the closed position.[18] That structural result explained data from pH−rate profiles and kinetic isotope effects indicating that general acid catalysis was lost in the W354F mutant. Those results were surprising in light of the fact that the corresponding mutation to the conserved tryptophan in the WPD loop of PTP1B has only a minor effect on rate and does not compromise general acid catalysis.

In this work, the reduced rates and pH−rate profiles of the W354H and W354Y mutants are also consistent with WPD loops that cannot achieve the catalytically functional closed position needed for general acid catalysis. The pH−rate profile of WT YopH (Figure 3) shows the bell curve characteristic of PTPs, which, on the acidic limb, gives the pK_a of the cysteine nucleophile and, on the basic limb, gives the pK_a of the aspartic acid.[52] The closed WDP loop in WT structures with bound oxyanion inhibitors shows the general acid D356 within hydrogen bonding distance of an apical oxygen of the bound ligand corresponding to the position of the scissile oxygen of the tyrosine leaving group in the first step of the reaction. When the WPD loop is in the quasi-open position seen in the W354H and W354Y mutants, the D356 side chain is outside of hydrogen bonding range and can no longer perform as a general acid (Figure S4).

Divanadate Species Are Consistently Observed in Crystal Structures of Loop-Impaired YopH, but Never in Native PTPs. Vanadate modulates a number of biological processes, generating interest in the origin of its interactions with proteins.[54−61] In particular, vanadate is a potent inhibitor of many phosphatases, and its insulin mimetic effect is ascribed to its inhibition of PTPs.[62,63] An understanding of these effects is complicated by the tendency of vanadate to oligomerize.[64] Inhibitory effects are observed under conditions where vanadate is primarily oligomerized and the monomer is a minor form.[56,64] The reaction of vanadate with organic molecules containing hydroxyl groups to form esters is well-known. Nuclear magnetic resonance has been used to document the formation of binary and ternary complexes with monodentate and bidentate ligands in aqueous solution. Such species are of variable stability and exist in an equilibrium that is pH-dependent. Even vanadate tetramers have been implicated as important inhibitory species in vitro and in vivo.[56,64−66]

Even though protein crystallization conditions often require vanadate concentrations that would primarily result in oligomeric species, such structures almost exclusively show monomeric vanadate at the active site. In WT YopH vanadate structures, bound vanadate is a pentacoordinated monomer that resembles the transition state for phosphoryl transfer. This

DOI: 10.1021/acs.biochem.5b00496
Biochemistry XXXX, XXX, XXX−XXX

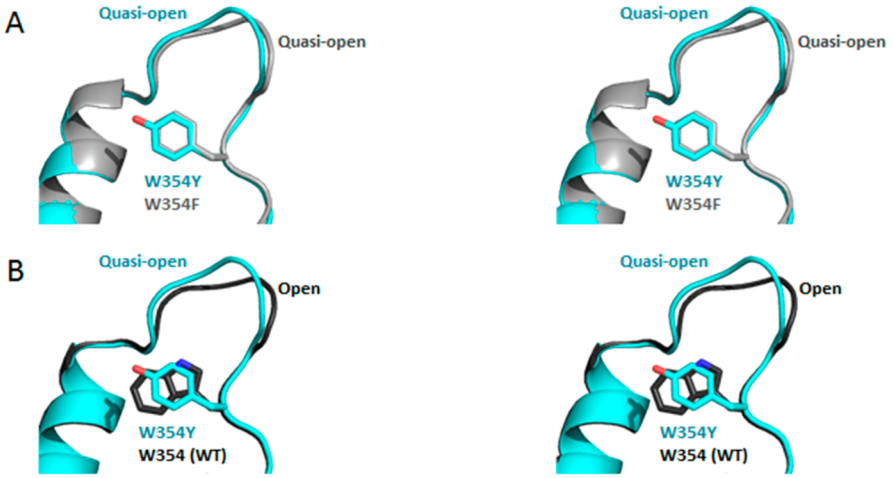

Figure 6. Stereo figure of the superposition of the YopH W354Y mutant with published structures, comparing the position of the tyrosine side chain with phenylalanine and tryptophan. (A) W354Y (cyan) overlaid with the W354F structure (gray, PDB entry 3F9B). The tyrosine side chain occupies the same position as phenylalanine. (B) W354Y (cyan) overlaid with WT YopH in the open-loop position (black, PDB entry 1YPT). The tyrosine is coplanar with the indole side chain of tryptophan.

has been attributed to the facile interconvertability of different vanadate species in solution, and the ability of the active sites of phosphatases to selectively stabilize the monomeric form.[67] However, active PTPs should catalyze the decomposition of any dimeric forms that bind in solution, using the same mechanism and catalytic groups as for phosphomonoester hydrolysis.[68] This would leave behind the monomeric forms that are routinely observed.

When crystallized in the presence of vanadate, all three YopH mutants (W354F, W354H, and W354Y) show the presence of a dimeric form of vanadate. Kinetic and crystallographic evidence is consistent with the WPD loop impaired such that general acid D356 does not reach the active site. In contrast, the analogous W354F mutant of PTP1B remains fully functional,[17] and crystals grown in the presence of vanadate show the monomeric form at the active site.[69] This is not surprising, because a functional general acid would catalyze the decomposition by hydrolysis of the dimeric forms observed in the loop-compromised mutants. The loss of general acid catalysis permits the trapping of a form of vanadate that is known to exist in solution, and which the structures demonstrate is clearly able to bind effectively to the active site. Thus, the monomeric form of vanadate typically observed in crystal structures of phosphatases is not the only form and may not be the major form that binds to the active site in solution. Phosphatase complexes with vanadate are typically grown under conditions where oligomeric forms of vanadate predominate. These results indicate that inhibition by monomeric vanadate is probably not the only contributor to the biological effects of vanadate via enzyme inhibition.

The importance of local medium effects in stabilizing particular vanadate species is another important consideration.[19,20] These factors likely contribute to the formation and observation of the divanadate glycerol ester observed in the crystal structures of the W354H and W354Y mutants. Glycerol is added after crystals had grown, as a cryoprotection for data collection at cryogenic temperatures (100 K). Vanadate is known to form esters with hydroxyl-bearing molecules in solution. A number of small molecule divanadate esters are known from the Cambridge database that are analogous to the glycerol esters found in this study, showing that such species can form in solution in a manner independent of an enzymatic active site. Kinetic data show no indication of a synergistic inhibitory effect on YopH activity between glycerol and vanadate. Therefore, the esters observed in the crystals most likely formed at the active site where divanadate was already bound.

Two of the small molecule precedents for analogous polyhydroxy esters with bridged vanadium(V) species, compound 1 (Figure 4E and Figure S1)[70] and compound 2 (Figure S2),[71] were used in a computational analysis to assess how the protein environment affects the bonding and charges.

Electronic Nature of the Divanadate Complexes. Among vanadate phosphatase X-ray structures, divanadate is uniquely found in the W354 mutants of YopH. The local environment can significantly affect the bonding and stability of vanadate species.[19,20] The active site of the phosphatase VHZ allowed stabilization and identification of metavanadate.[68] This led to a computational investigation of the bonding interactions within this ligand and how it interacts with the active. The structures of the divanadate moieties are very similar in structure, but one significant difference noted between the atomic charges of the simple divanadate complex in W354F and the glycerol ester in W354Y is the more negative charge on the cysteine sulfur atom in W354F. In both complexes, the sulfur is an apical ligand to the vanadium atom at the bottom of the active site. The higher negative charge in W354F means this interaction is more ionic in character. Similarly, both of the bridging oxygen atoms, O3 and O4, are more negative in this complex. This is possibly a stabilizing response to the larger negative charge on sulfur, as O3 is coordinated to two backbone amide hydrogen atoms. The coordinated glycerol has the effect of reducing the degree of polarization of these atoms.

A gap in electron density is evident between O7 and V2 of the glycerol complex. The computational analysis shows that this bond is highly ionic with 17% of electron density residing on V2 and 83% on O7. Under all circumstances, a bond was found between O7 and the terminal glycerol carbon, irrespective of basis set, with a high population.

The effectiveness of hydrogen bonding in the protein environment in stabilizing charge can be seen in the comparative partial charges on O5 and O6 in the divanadate

DOI: 10.1021/acs.biochem.5b00496
Biochemistry XXXX, XXX, XXX−XXX

glycerol complex. The charge is higher on the atom modeled as protonated (O5) than on O6, which is hydrogen bonded to two backbone amide hydrogens. The small molecule analogues were found to be very similar to their protein-bound counterparts. In particular, the partial charges on the vanadium atoms closely resembled those of the model with a similar set of coordinated atoms. The vanadium atom coordinated to cysteine, V1, in both complexes has an atomic charge very similar to that of the symmetric model compound 1, in which each vanadium atom has four oxygens and one sulfur ligand. The outer vanadium atom, V2, has a higher partial positive charge, very similar to those in the compound 2 complex that has five oxygen ligands to each vanadium atom.

Origins of Impaired Loop Motion by Conservative Mutations to Trp354 in YopH. Mutation of the conserved tryptophan to phenylalanine disables general acid catalysis in YopH, but not PTP1B.[17] An examination of crystal structures reveals that, in both enzymes, loop closure is accompanied by a repositioning of the conserved indole side chain within a hydrophobic pocket.[18] In the complex with vanadate, the W179F mutant of PTP1B has the WPD loop in its normal closed position, and the ligand-free enzyme has an open WPD loop. In contrast, structures of the W354F YopH mutant show the WPD loop in the same quasi-open position regardless of whether an oxyanion is bound. It was proposed that the W354F mutation locked the WPD loop in YopH, resulting from steric clashes that would arise in a fully closed-loop conformation. The loop may not be locked in solution. The original mutation, as well as the mutations to His and Tyr reported here, may instead alter the energy landscape such that the quasi-open positions observed are the lowest-energy conformations and thus observed in crystals. There may be further loop motion retained in solution. However, the kinetic results make it clear that general acid catalysis is no longer operative in these mutants. If the loop is still able to close normally, it occurs too infrequently to contribute to catalysis. The absence of acid catalysis is inferred from loss of the basic limb of the pH−rate profile and confirmed using kinetic isotope effects in the original W354F mutant.[21]

Structures of the W354Y and W354H mutants were examined for the origins of hindered loop closure. Figure 6 shows the relative positioning of the Y354 side chain compared with the F354 mutant. Both mutants have WPD loops in similar positions, and the residue 354 side chains are in the same positions. The bottom panel of Figure 6 shows an overlay of W354Y with the open-loop conformation of native YopH. Figure 7 shows YopH in the closed-loop conformation superimposed with the W354Y and W354H mutants. In the quasi-open conformations of the mutants, the backbone carbonyl oxygen of residue 354 makes a hydrogen bond to the side chain of general acid D356. Upon loop closure in the native enzyme, this interaction is replaced with a hydrogen bond to an N−H of R409. The closed-loop conformation of the native enzyme is also stabilized by a hydrogen bond between the indole N−H and the backbone carbonyl of T358. None of the mutants can form this hydrogen bond.

Figure 8 shows a hypothetical position of the Y354 side chain in a closed-loop position of the enzyme. This orientation was obtained by assuming the same position of the backbone carbon chain and the first two carbons of the side chain, and coplanarity of the aromatic rings. The hydrogens of the six-membered ring would result in steric clashes in a fully closed-loop position. In addition, this conformation would place the phenolic oxygen atom 1.9 Å from the backbone carbonyl oxygen of T358. Both considerations would make it energeti-

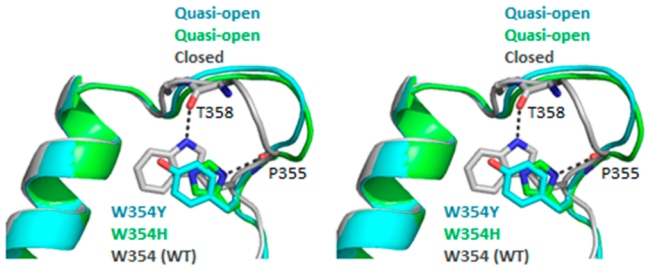

Figure 7. Comparison of the position of the side chains of YopH W354H (green) and W354Y (cyan), with the native YopH W354 (white) in the closed-loop position. The indole N−H of the native enzyme forms a hydrogen bond with the backbone carbonyl of T358 in the closed-loop conformation. The histidine imidazole ring in W354H superimposes well with the indole ring of the tryptophan when the native enzyme is in the open-loop position. A hydrogen bond is evident between the N−H of the imidazole ring and the backbone carbonyl of the residue P355, stabilizing the quasi-open conformation of this mutant. No such interaction is present in native YopH. In both structures, the backbone carbonyl of residue 354 hydrogen bonds to the side chain of P355. Upon loop closure in native YopH, this interaction is replaced by a hydrogen bond to the N−H of R409.

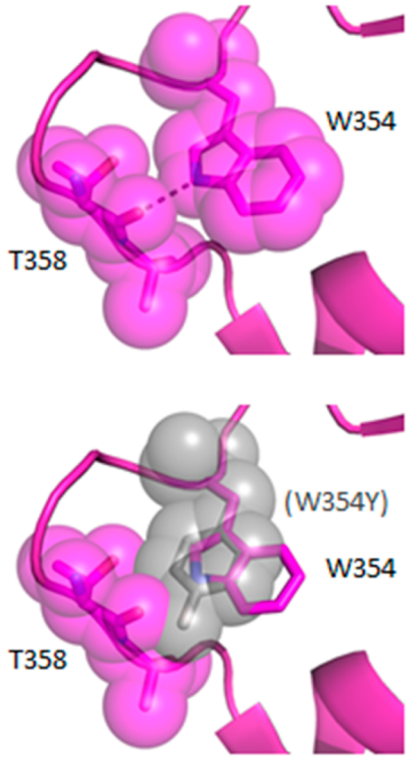

Figure 8. Full loop closure of the W354Y mutant would result in several steric clashes. The top panel shows a space-filling model of the WPD-loop-closed native YopH. The indole N−H of the native enzyme forms a hydrogen bond with the backbone carbonyl of T358. The bottom panel shows the predicted position of the W354Y side chain (gray) in the closed-loop position, assuming the residue backbone and the first two carbons of the side chain occupy the same positions as W354 of the native enzyme (purple). In addition to significant overlap involving carbon atoms on the six-membered ring, the phenolic oxygen would be ~1.9 Å from the backbone carbonyl oxygen of T358.

DOI: 10.1021/acs.biochem.5b00496
Biochemistry XXXX, XXX, XXX−XXX

cally unfavorable for the loop in W354Y to close in the manner seen in the native enzyme.

The phenylalanine and tyrosine mutants both place a six-membered ring in a position overlaying the five-membered indole ring of the native enzyme. The histidine mutant also exhibits a quasi-open loop, even though structural data show the five-membered imidazole ring superimposes well with the five-membered ring of indole in the open-loop position. However, the different regiochemistry of the N−H of the imidazole results in a hydrogen bond with the backbone carbonyl of P355. There is no analogous hydrogen bond in the native enzyme, with the closest analogy being the previously mentioned indole N−H hydrogen bond with T358 present in the closed conformation. This interaction will stabilize the quasi-open position and present a barrier to full loop closure.

CONCLUSIONS

The rates of WPD-loop movement have been shown to be variable among PTP family members and are correlated with their catalytic activities. Conservative mutations to noncatalytic residues in the loop have different effects in YopH compared to PTP1B. These results show that YopH is intolerant of any aromatic side chain at position 354 other than the indole found in the native enzyme. In all three mutants with other aromatic side chains, in crystal structures with vanadate bound the WPD loop is found in a similar, quasi-open position that does not permit acid catalysis.

The results show that, unlike PTP1B, YopH is completely intolerant of even conservative substitutions to the tryptophan side chain in the WPD loop. The vanadate-complexed structures provide further support, beyond the single previous instance, for the ability of divanadate to bind to the active site of PTPs. Although crystal structures of vanadate bound to native phosphatases show only the monomeric form, vanadate has significant biological effects and is a potent phosphatase inhibitor under conditions where oligomeric forms are dominant. The consistent finding of a dimeric form in all three WPD-loop-compromised YopH mutants shows the single previous instance was not an anomaly and suggests that oligomeric forms of vanadate and their esters can compete for PTP active sites. More hydrogen bonds are observed with the divanadate species than the monomer. A native PTP would cleave such forms, leaving behind the monomeric vanadate typically observed. The initial binding of higher-order vanadate oligomers to phosphatases likely contributes to their inhibitory activity, before they are hydrolyzed to the monomeric form observed in crystal structures.

ASSOCIATED CONTENT

Supporting Information

The Supporting Information is available free of charge on the ACS Publications website at DOI: 10.1021/acs.biochem.5b00496.

Full list of electronic structure parameters characterizing the vanadate complexes from W354Y and W354H and small molecule analogues, kinetic plots showing the effect of glycerol on the inhibition of W354H YopH by vanadate, and a figure comparing the position of general acid D356 in the catalytically active, WPD-loop-closed conformation of native YopH and in the quasi-open-loop position of W354Y (PDF)

AUTHOR INFORMATION

Corresponding Authors

*E-mail: alvan.hengge@usu.edu. Phone: (435) 797-3442. Fax: (435) 797-3390.

*E-mail: sean.johnson@usu.edu. Phone: (435) 797-2089. Fax: (435) 797-3390.

Funding

This work was supported by National Institutes of Health Grant R01GM47297 (A.C.H.), National Science Foundation (NSF) MRI Grant DBI1228874 (S.J.J.), and an Alfred P. Sloan Fellowship and NSF CAREER Award CHE-1351968 (A.N.A.).

Notes

The authors declare no competing financial interest.

ACKNOWLEDGMENTS

We thank Dr. Tiago Brandao for advice on mutagenesis and crystallization conditions in the early stages of this project and Kyle Berg for assistance in obtaining kinetic data.

ABBREVIATIONS

PTP, protein tyrosine phosphatase; YopH, *Yersinia* outer protein H; IPTG, isopropyl *β*-D-1-thiogalactopyranoside; DTT, dithiothreitol; *p*-NPP, *p*-nitrophenyl phosphate; HEPES, 4-(2-hydroxyethyl)-1-piperazineethanesulfonic acid; PEG, polyethylene glycol; EDTA, ethylenediaminetetraacetic acid.

REFERENCES

(1) Hunter, T. (1995) Protein Kinases and Phosphatases: The Yin and Yang of Protein Phosphorylation and Signaling. *Cell 80*, 225−236.

(2) Jackson, M. D., and Denu, J. M. (2001) Molecular reactions of protein phosphatases–insights from structure and chemistry. *Chem. Rev. 101*, 2313−2340.

(3) Burke, T. R., Jr., and Zhang, Z. Y. (1998) Protein-tyrosine phosphatases: structure, mechanism, and inhibitor discovery. *Biopolymers 47*, 225−241.

(4) Alonso, A., Sasin, J., Bottini, N., Friedberg, I., Friedberg, I., Osterman, A., Godzik, A., Hunter, T., Dixon, J., and Mustelin, T. (2004) Protein tyrosine phosphatases in the human genome. *Cell 117*, 699−711.

(5) Brubaker, R. R. (1991) Factors promoting acute and chronic diseases caused by yersiniae. *Clin. Microbiol. Rev. 4*, 309−324.

(6) Zhang, Z. Y., Thieme-Sefler, A. M., Maclean, D., McNamara, D. J., Dobrusin, E. M., Sawyer, T. K., and Dixon, J. E. (1993) Substrate specificity of the protein tyrosine phosphatases. *Proc. Natl. Acad. Sci. U. S. A. 90*, 4446−4450.

(7) Zhang, Z.-Y., Clemens, J. C., Schubert, H. L., Stuckey, J. A., Fischer, M. W. F., Hume, D. M., Saper, M. A., and Dixon, J. E. (1992) Expression, purification, and physicochemical characterization of a recombinant Yersinia protein tyrosine phosphatase. *J. Biol. Chem. 267*, 23759−23766.

(8) Lad, C., Williams, N. H., and Wolfenden, R. (2003) The rate of hydrolysis of phosphomonoester dianions and the exceptional catalytic proficiencies of protein and inositol phosphatases. *Proc. Natl. Acad. Sci. U. S. A. 100*, 5607−5610.

(9) Zhang, Z.-Y. (1997) Structure, mechanism and specificity of protein-tyrosine phosphatases. *Curr. Top. Cell. Regul. 35*, 21−68.

(10) Zhang, Z.-Y., Wang, Y., and Dixon, J. E. (1994) Dissecting the catalytic mechanism of protein-tyrosine phosphatases. *Proc. Natl. Acad. Sci. U. S. A. 91*, 1624−1627.

(11) Barford, D., Flint, A. J., and Tonks, N. K. (1994) Crystal structure of human protein tyrosine phosphatase 1B. *Science 263*, 1397−1404.

(12) Stuckey, J. A., Schubert, H. L., Fauman, E. B., Zhang, Z.-Y., Dixon, J. E., and Saper, M. A. (1994) Crystal structure of *Yersinia*

DOI: 10.1021/acs.biochem.5b00496
Biochemistry XXXX, XXX, XXX−XXX

protein phosphatase at 2.5 angstroms and the complex with tungstate. *Nature 370*, 571−575.
(13) Fauman, E. B., Yuvaniyama, C., Schubert, H., Stuckey, J. A., and Saper, M. A. (1996) The x-ray crystal structures of *Yersinia* tyrosine phosphatase with bound tungstate and nitrate. Mechanistic implications. *J. Biol. Chem. 271*, 18780−18788.
(14) Groves, M. R., Yao, Z. J., Roller, P. P., Burke, T. R., Jr., and Barford, D. (1998) Structural basis for inhibition of the protein tyrosine phosphatase 1B by phosphotyrosine peptide mimetics. *Biochemistry 37*, 17773−17783.
(15) Schubert, H. L., Fauman, E. B., Stuckey, J. A., Dixon, J. E., and Saper, M. A. (1995) A ligand-induced conformational change in the *Yersinia* protein tyrosine phosphatase. *Protein Sci. 4*, 1904−1913.
(16) Whittier, S. K., Hengge, A. C., and Loria, J. P. (2013) Conformational motions regulate phosphoryl transfer in related protein tyrosine phosphatases. *Science 341*, 899−903.
(17) Brandao, T. A., Johnson, S. J., and Hengge, A. C. (2012) The molecular details of WPD-loop movement differ in the protein-tyrosine phosphatases YopH and PTP1B. *Arch. Biochem. Biophys. 525*, 53−59.
(18) Brandao, T. A. S., Robinson, H., Johnson, S. J., and Hengge, A. C. (2009) Impaired Acid Catalysis by Mutation of a Protein Loop Hinge Residue in a YopH Mutant Revealed by Crystal Structures. *J. Am. Chem. Soc. 131*, 778−786.
(19) Crans, D. C., Baruah, B., Ross, A., and Levinger, N. E. (2009) Impact of confinement and interfaces on coordination chemistry: Using oxovanadate reactions and proton transfer reactions as probes in reverse micelles. *Coord. Chem. Rev. 253*, 2178−2185.
(20) Crans, D. C., Schoeberl, S., Gaidamauskas, E., Baruah, B., and Roess, D. A. (2011) Antidiabetic vanadium compound and membrane interfaces: interface-facilitated metal complex hydrolysis. *JBIC, J. Biol. Inorg. Chem. 16*, 961−972.
(21) Hoff, R. H., Hengge, A. C., Wu, L., Keng, Y. F., and Zhang, Z. Y. (2000) Effects on general acid catalysis from mutations of the invariant tryptophan and arginine residues in the protein tyrosine phosphatase from Yersinia. *Biochemistry 39*, 46−54.
(22) Gordon, J. A. (1991) Use of vanadate as protein-phosphotyrosine phosphatase inhibitor. *Methods Enzymol. 201*, 477−482.
(23) Gordon, J. A. (1991) Use of Vanadate as Protein-Phosphotyrosine Phosphatase Inhibitor. *Methods Enzymol. 201*, 477−482.
(24) Otwinowski, Z., and Minor, W. (1997) Processing of X-ray diffraction data collected in oscillation mode. *Methods Enzymol. 276*, 307−326.
(25) Mccoy, A. J., Grosse-Kunstleve, R. W., Adams, P. D., Winn, M. D., Storoni, L. C., and Read, R. J. (2007) Phaser crystallographic software. *J. Appl. Crystallogr. 40*, 658−674.
(26) Winn, M. D., Ballard, C. C., Cowtan, K. D., Dodson, E. J., Emsley, P., Evans, P. R., Keegan, R. M., Krissinel, E. B., Leslie, A. G., McCoy, A., McNicholas, S. J., Murshudov, G. N., Pannu, N. S., Potterton, E. A., Powell, H. R., Read, R. J., Vagin, A., and Wilson, K. S. (2011) Overview of the CCP4 suite and current developments. *Acta Crystallogr., Sect. D: Biol. Crystallogr. 67*, 235−242.
(27) Adams, P. D., Afonine, P. V., Bunkoczi, G., Chen, V. B., Davis, I. W., Echols, N., Headd, J. J., Hung, L. W., Kapral, G. J., Grosse-Kunstleve, R. W., McCoy, A. J., Moriarty, N. W., Oeffner, R., Read, R. J., Richardson, D. C., Richardson, J. S., Terwilliger, T. C., and Zwart, P. H. (2010) PHENIX: a comprehensive Python-based system for macromolecular structure solution. *Acta Crystallogr., Sect. D: Biol. Crystallogr. 66*, 213−221.
(28) Stuckey, J. A., Schubert, H. L., Fauman, E. B., Zhang, Z. Y., Dixon, J. E., and Saper, M. A. (1994) Crystal-Structure of Yersinia Protein-Tyrosine-Phosphatase at 2.5-Angstrom and the Complex with Tungstate. *Nature 370*, 571−575.
(29) Emsley, P., Lohkamp, B., Scott, W. G., and Cowtan, K. (2010) Features and Development of Coot. *Acta Crystallogr., Sect. D: Biol. Crystallogr. 66*, 486−501.
(30) Afonine, P. V., Grosse-Kunstleve, R. W., Echols, N., Headd, J. J., Moriarty, N. W., Mustyakimov, M., Terwilliger, T. C., Urzhumtsev, A., Zwart, P. H., and Adams, P. D. (2012) Towards automated crystallographic structure refinement with phenix.refine. *Acta Crystallogr., Sect. D: Biol. Crystallogr. 68*, 352−367.
(31) Davis, I. W., Leaver-Fay, A., Chen, V. B., Block, J. N., Kapral, G. J., Wang, X., Murray, L. W., Arendall, W. B., 3rd, Snoeyink, J., Richardson, J. S., and Richardson, D. C. (2007) MolProbity: all-atom contacts and structure validation for proteins and nucleic acids. *Nucleic Acids Res. 35*, W375−383.
(32) DeLano, W. L. (2007) *The PyMOL Molecular Graphics System*, version 1.3, DeLano Scientific LLC, Palo Alto, CA.
(33) Pettersen, E. F., Goddard, T. D., Huang, C. C., Couch, G. S., Greenblatt, D. M., Meng, E. C., and Ferrin, T. E. (2004) UCSF Chimera–a visualization system for exploratory research and analysis. *J. Comput. Chem. 25*, 1605−1612.
(34) Hanwell, M. D., Curtis, D. E., Lonie, D. C., Vandermeersch, T., Zurek, E., and Hutchison, G. R. (2012) Avogadro: an advanced semantic chemical editor, visualization, and analysis platform. *J. Cheminf. 4*, 17.
(35) Carpenter, J. E., and Weinhold, F. (1988) Analysis of the geometry of the hydroxymethyl radical by the "different hybrids for different spins" natural bond orbital procedure. *J. Mol. Struct.: THEOCHEM 169*, 41−62.
(36) Foster, J. P., and Weinhold, F. (1980) Natural hybrid orbitals. *J. Am. Chem. Soc. 102*, 7211−7218.
(37) Reed, A. E., Curtiss, L. A., and Weinhold, F. (1988) Intermolecular interactions from a natural bond orbital, donor-acceptor viewpoint. *Chem. Rev. 88*, 899−926.
(38) Reed, A. E., and Weinhold, F. (1983) Natural bond orbital analysis of near Hartree−Fock water dimer. *J. Chem. Phys. 78*, 4066.
(39) Becke, A. D. (1993) Density-Functional Thermochemistry 0.3. The Role of Exact Exchange. *J. Chem. Phys. 98*, 5648−5652.
(40) Parr, R. G., and Yang, W. (1989) *Density-functional theory of atoms and molecules*, Oxford University Press, Oxford, U.K.
(41) Perdew, J. P., Chevary, J. A., Vosko, S. H., Jackson, K. A., Pederson, M. R., Singh, D. J., and Fiolhais, C. (1992) Atoms, Molecules, Solids, and Surgaces: Applications of the Generalized Gradient Approximation for Exchange and Correlation. *Phys. Rev. B: Condens. Matter Mater. Phys. 46*, 6671−6687.
(42) Schafer, A., Huber, C., and Ahlrichs, R. (1994) Fully Optimized Contracted Gaussian-Basis Sets of Triple Zeta Valence Quality for Atoms Li to Kr. *J. Chem. Phys. 100*, 5829−5835.
(43) *Turbomole* (2007) University of Karlsruhe and Forschungszentrum Karlsruhe GmbH, Karlsruhe, Germany.
(44) Weigend, F., and Ahlrichs, R. (2005) Balanced basis sets of split valence, triple zeta valence and quadruple zeta valence quality for H to Rn: Design and assessment of accuracy. *Phys. Chem. Chem. Phys. 7*, 3297−3305.
(45) Weigend, F., Haser, M., Patzelt, H., and Ahlrichs, R. (1998) RI-MP2: optimized auxiliary basis sets and demonstration of efficiency. *Chem. Phys. Lett. 294*, 143−152.
(46) Von Arnim, M., and Ahlrichs, R. (1998) Performance of parallel TURBOMOLE for density functional calculations. *J. Comput. Chem. 19*, 1746−1757.
(47) Sierka, M., Hogekamp, A., and Ahlrichs, R. (2003) Fast evaluation of the Coulomb potential for electron densities using multipole accelerated resolution of identity approximation. *J. Chem. Phys. 118*, 9136−9148.
(48) Grimme, S. (2004) Calculation of the electronic spectra of large molecules. *Rev. Comp Ch 20*, 153−218.
(49) Klamt, A., and Schuurmann, G. (1993) Cosmo - a New Approach to Dielectric Screening in Solvents with Explicit Expressions for the Screening Energy and Its Gradient. *J. Chem. Soc., Perkin Trans. 2*, 799−805.
(50) Frisch, M. J., Pople, J. A., and Binkley, J. S. (1984) Self-Consistent Molecular Orbital Methods 25. Supplementary Functions for Gaussian Basis Sets. *J. Chem. Phys. 80*, 3265−3269.

DOI: 10.1021/acs.biochem.5b00496
Biochemistry XXXX, XXX, XXX−XXX

(51) Frisch, M. J., Trucks, G. W., Schlegel, H. B., Scuseria, G. E., Robb, M. A., Cheeseman, J. R., Scalmani, G., Barone, V., Mennucci, B., Petersson, G. A., Nakatsuji, H., Caricato, M., Li, X., Hratchian, H. P., Izmaylov, A. F., Bloino, J., Zheng, G., Sonnenberg, J. L., Hada, M., Ehara, M., Toyota, K., Fukuda, R., Hasegawa, J., Ishida, M., Nakajima, T., Honda, Y., Kitao, O., Nakai, H., Vreven, T., Montgomery, J. A., Jr., Peralta, J. E., Ogliaro, F., Bearpark, M., Heyd, J. J., Brothers, E., Kudin, K. N., Staroverov, V. N., Kobayashi, R., Normand, J., Raghavachari, K., Rendell, A., Burant, J. C., Iyengar, S. S., Tomasi, J., Cossi, M., Rega, N., Millam, N. J., Klene, M., Knox, J. E., Cross, J. B., Bakken, V., Adamo, C., Jaramillo, J., Gomperts, R., Stratmann, R. E., Yazyev, O., Austin, A. J., Cammi, R., Pomelli, C., Ochterski, J. W., Martin, R. L., Morokuma, K., Zakrzewski, V. G., Voth, G. A., Salvador, P., Dannenberg, J. J., Dapprich, S., Daniels, A. D., Farkas, Ö., Foresman, J. B., Ortiz, J. V., Cioslowski, J., and Fox, D. J. (2009) *Gaussian 09*, Gaussian, Inc., Wallingford, CT.

(52) Keng, Y.-F., Wu, L., and Zhang, Z.-Y. (1999) Probing the function of the invariant tryptophan in the flexible loop of protein-tyrosine phosphatases. *Eur. J. Biochem. 259*, 809−814.

(53) Bernstein, F. C., Koetzle, T. F., Williams, G. J., Meyer, E. F., Jr., Brice, M. D., Rodgers, J. R., Kennard, O., Shimanouchi, T., and Tasumi, M. (1977) The Protein Data Bank: a computer-based archival file for macromolecular structures. *J. Mol. Biol. 112*, 535−542.

(54) Bishayee, A., Waghray, A., Patel, M. A., and Chatterjee, M. (2010) Vanadium in the detection, prevention and treatment of cancer: the in vivo evidence. *Cancer Lett. 294*, 1−12.

(55) Cam, M. C., Brownsey, R. W., and McNeill, J. H. (2000) Mechanisms of vanadium action: insulin-mimetic or insulin-enhancing agent? *Can. J. Physiol. Pharmacol. 78*, 829−847.

(56) Crans, D. C., Smee, J. J., Gaidamauskas, E., and Yang, L. (2004) The chemistry and biochemistry of vanadium and the biological activities exerted by vanadium compounds. *Chem. Rev. 104*, 849−902.

(57) Evangelou, A. M. (2002) Vanadium in cancer treatment. *Critical reviews in oncology/hematology 42*, 249−265.

(58) Heyliger, C. E., Tahiliani, A. G., and McNeill, J. H. (1985) Effect of vanadate on elevated blood glucose and depressed cardiac performance of diabetic rats. *Science 227*, 1474−1477.

(59) Rubinson, K. A. (1981) Concerning the form of biochemically active vanadium. *Proc. R. Soc. London, Ser. B 212*, 65−84.

(60) Tsiani, E., Bogdanovic, E., Sorisky, A., Nagy, L., and Fantus, I. G. (1998) Tyrosine phosphatase inhibitors, vanadate and pervanadate, stimulate glucose transport and GLUT translocation in muscle cells by a mechanism independent of phosphatidylinositol 3-kinase and protein kinase C. *Diabetes 47*, 1676−1686.

(61) Tsiani, E., and Fantus, I. G. (1997) Vanadium Compounds Biological Actions and Potentialas Pharmacological Agents. *Trends Endocrinol. Metab. 8*, 51−58.

(62) Bhattacharyya, S., and Tracey, A. S. (2001) Vanadium(V) complexes in enzyme systems: aqueous chemistry, inhibition and molecular modeling in inhibitor design. *J. Inorg. Biochem. 85*, 9−13.

(63) Shechter, Y. (1990) Insulin-mimetic effects of vanadate. Possible implications for future treatment of diabetes. *Diabetes 39*, 1−5.

(64) Crans, D. C., Willging, E. M., and Butler, S. R. (1990) Vanadate Tetramer as the Inhibiting Species in Enzyme Reactions in Vitro and in Vivo. *J. Am. Chem. Soc. 112*, 427−432.

(65) Crans, D. C. (1994) Enzyme interactions with labile oxovanadates and other polyoxometalates. *Comments Inorg. Chem. 16*, 35−76.

(66) Crans, D. C. (2005) Fifteen years of dancing with vanadium. *Pure Appl. Chem. 77*, 1497−1527.

(67) Crans, D. C., Rithner, C. D., and Theisen, L. A. (1990) Application of Time-Resolved V-51 2d Nmr for Quantitation of Kinetic Exchange Pathways between Vanadate Monomer, Dimer, Tetramer, and Pentamer. *J. Am. Chem. Soc. 112*, 2901−2908.

(68) Kuznetsov, V. I., Alexandrova, A. N., and Hengge, A. C. (2012) Metavanadate at the active site of the phosphatase VHZ. *J. Am. Chem. Soc. 134*, 14298−14301.

(69) Brandao, T. A., Hengge, A. C., and Johnson, S. J. (2010) Insights into the reaction of protein tyrosine phosphatase 1B. Crystal structures for transition-state analogs of both catalytic steps. *J. Biol. Chem. 285*, 15874−15883.

(70) Bhattacharyya, S., Batchelor, R. J., Einstein, F. W. B., and Tracey, A. S. (1999) Crystal structure and solution studies of the product of the reaction of beta-mercaptoethanol with vanadate. *Can. J. Chem. 77*, 2088−2094.

(71) Zhang, B. Y., Zhang, S. W., and Wang, K. (1996) Synthesis, characterization and crystal structure of cyclic vanadate complexes with monosaccharide derivatives having a free adjacent diol system. *J. Chem. Soc., Dalton Trans.*, 3257−3263.

DOI: 10.1021/acs.biochem.5b00496
Biochemistry XXXX, XXX, XXX−XXX